

Magnetic phase diagram of HoFeO₃ by neutron diffraction

A. K. Ovsianikov^{1,2}, O.V. Usmanov¹, I. A. Zobkalo¹, V. Hutanu^{2,3}, S.N. Barilo⁴, N.A. Liubachko⁴, K.A. Shaykhutdinov^{5,6}, K. Yu Terentjev⁵, S.V. Semenov^{5,6}, T. Chatterji⁷, M. Meven^{2,3}, P. J. Brown⁷, G. Roth², L. Peters², H. Deng³, A. Wu⁸.

¹ Petersburg Nuclear Physics Institute by B.P. Konstantinov of NRC «Kurchatov Institute», 188300 Gatchina, Russia.

² Institute of Crystallography, RWTH Aachen University, 52066 Aachen, Germany

³ Jülich Centre for Neutron Science at Heinz Maier-Leibnitz Zentrum, Lichtenbergstrae 1, 85747 Garching, Germany

⁴ Scientific-Practical Materials Research Centre NAS of Belarus, 19 P. Brovki str., Minsk, 220072, Belarus;

⁵ Kirensky Institute of Physics, Federal Research Center, Krasnoyarsk 660036, Russia

⁶ Siberian Federal University, Krasnoyarsk, 660071, Russia

⁷ Institut Laue-Langevin, 71 Avenue des Martyrs, CS 20156 - 38042 Grenoble Cedex 9, France

⁸ Institute of Ceramic, Chinese Academy of Sciences, Shanghai 200050, China

Abstract

Neutron diffraction studies of HoFeO₃ single crystal were performed under external magnetic fields. The interplay between the external magnetic field, Dzyaloshinsky-Moria antisymmetric exchange and isotropic exchange interactions between Fe and Ho sublattice and inside Fe sublattice provides a rich phase diagram. As the result of the balance of exchange interactions inside crystal and external magnetic field we found 8 different magnetic phases, produced or suppressed by the field.

Introduction

Rare-earth orthoferrites $R\text{FeO}_3$ studies have been known since the 60s of the last century [1 – 3]. These compounds belong to orthorhombic $Pnma$ space group and have high Neel temperatures $T_N = 620 - 740$ K. Below T_N iron subsystem orders antiferromagnetically with a weak ferromagnetic component. With temperature decrease, influence of the R ion leads to spin-reorientation (SR) transitions, which take place in a case of magnetic rare-earth ions. There is no such transitions for non-magnetic ions $R = Y, La, Lu$ [4]. The number and features of SR transitions could be different for different magnetic R ions, as well as temperatures T_{SR} . Temperature range of spin-reorientation transitions lasts from $T_{SR} = 37$ K for DyFeO₃ [5] to $T_{SR} = 480$ K for SmFeO₃ [6]. For compounds with $R = Dy, Sm, Tm, Er, Yb$ the only one SR transition reported and in TmFeO₃ and ErFeO₃ it goes through an intermediate mixed phase [7, 8]. Several SR transitions were detected in crystals with $R = Ho, Tb$ [9, 10]. Spontaneous ordering of the rare-earth sublattice takes place below $T_{NR} \sim 10$ K. Thus, family of rare-earth orthoferrites is a good example to study interaction between systems included $3d$ and $4f$ ions.

Interest to these compounds increased greatly after the prediction and subsequent discovery of their multiferroic properties. Symmetry analysis showed that orthoferrites may have ferroelectric polarization at temperatures below T_{NR} [11]. Indeed, the experiments have confirmed the presence of polarization below the magnetic ordering $T_{NR} = 5 - 10$ K in DyFeO₃ and GdFeO₃ [5, 12]. However, lately electric polarization in DyFeO₃ was observed at higher

temperature, around $T_{SR} = 50 - 60$ K [13]. In HoFeO_3 spontaneous electric polarization emerges at ~ 210 K [14]. In other orthoferrites like SmFeO_3 , YFeO_3 and LuFeO_3 , electric polarization was reported even at room temperature [15 – 17]. This brings these compounds close to being useful for potential applications in switching elements, sensors, memory and other advanced technical devices with low energy consumption. The mechanism leading to the emergence of ferroelectric polarization at high temperatures in $R\text{FeO}_3$ compounds is not understood. Dzyaloshinskii-Moriya interaction (DMI) [18, 19] which leads to weak ferromagnetism in Fe^{3+} sublattice could be regarded as one of the possible reasons of polarization. Because the distortion of oxygen octahedral leads to broken locally symmetric.

On the other hand, orthoferrites $R\text{FeO}_3$ show interesting anisotropic magnetocaloric phenomena. Magnetocaloric effect (MCE) describes the temperature change of magnetic materials in an adiabatic process caused by magnetic entropy change ΔS_M under external magnetic field. In TmFeO_3 entropy change ΔS_M has maximum ~ 12 J/kg K at the temperature 17 K under field 7 T along c axis; in TbFeO_3 ΔS_M reaches value of ~ 25 J/kg K at ~ 12 K in field 7 T along a axis [20]. This is, most likely, due to spin orientation transition in Fe subsystems. In HoFeO_3 entropy change ΔS_M has some extremums with values equal to 9 J/kg K at temperature $T = 53$ K, $\Delta S_M = 15$ J/kg K and $\Delta S_M = 18$ J/kg K in the external field of 7 T at temperatures $T = 10$ K and $T = 3$ K respectively [21], where the first peak also associated with spin orientation transition in Fe subsystems, while second and third ones apparently could be associated with some processes inside the holmium subsystem. Thus, this situation provides interest to study the phase diagram of HoFeO_3 in external magnetic fields. This will give a better understanding of the processes inside Ho subsystem, which provide these entropy jumps ΔS_M . In addition, external magnetic field will lead to changes of energy balance and will influence on exchange interaction and anisotropy inside holmium and iron subsystems.

Crystal structure of HoFeO_3 is described by space group #62 IT, $Pnma$ (or $Pbnm$ in another setting). Below $T_N = 647$ K Fe^{3+} sublattice has antiferromagnetic order with the strongest component along c -axis, and weak ferromagnetic component along b axis [1, 9]. As it was observed recently, compound has two spin-orientation transition at $T_{SR1} = 53$ K where moments of Fe^{3+} ions rotate in plane from c axis to a axis and at $T_{SR2} = 35$ K where strongest component of magnetic moments directed along b axis [9]. Ho^{3+} ordering takes place at temperature $T_{NR} \approx 4$ K [22 – 24].

Experimental

High quality single crystals of HoFeO_3 used for the neutron and magnetic studies have been grown using fluxed melt method [25, 26] and optical floating zone technique using FZ-4000 (Crystal Systems Corporation) installation. Crystal with dimensions $5 \times 4 \times 6$ mm³ was used for neutron studies. The orientation of the crystals obtained was controlled using Laue technique, the typical image of X-ray Laue is presented (Fig. 1). For the macroscopic and X-Ray measurements the samples from the same technology cycle were used. X-Ray studies were performed at Rigaku SmartLab diffractometer at PNPI. Measurements of the magnetic properties were carried out at the Krasnoyarsk Regional Center of Research Equipment of Federal Research Center «Krasnoyarsk Science Center SB RAS» on the vibrating sample magnetometers Quantum Design PPMS – 9T and Lakeshore VSM 8604.

Neutron diffraction experiments were performed at MLZ on the polarized neutron diffractometer POLI [27, 28]. Sample was mounted in 8 T cryomagnet, where it was fixed on the

sample stick with the glue from two sides and mechanically clamped with stronger tightening between two plates to prevent rotates along field at low temperature. In these measurements crystal b -axis was oriented vertically, while a and c axes were laying in horizontal scattering plane.

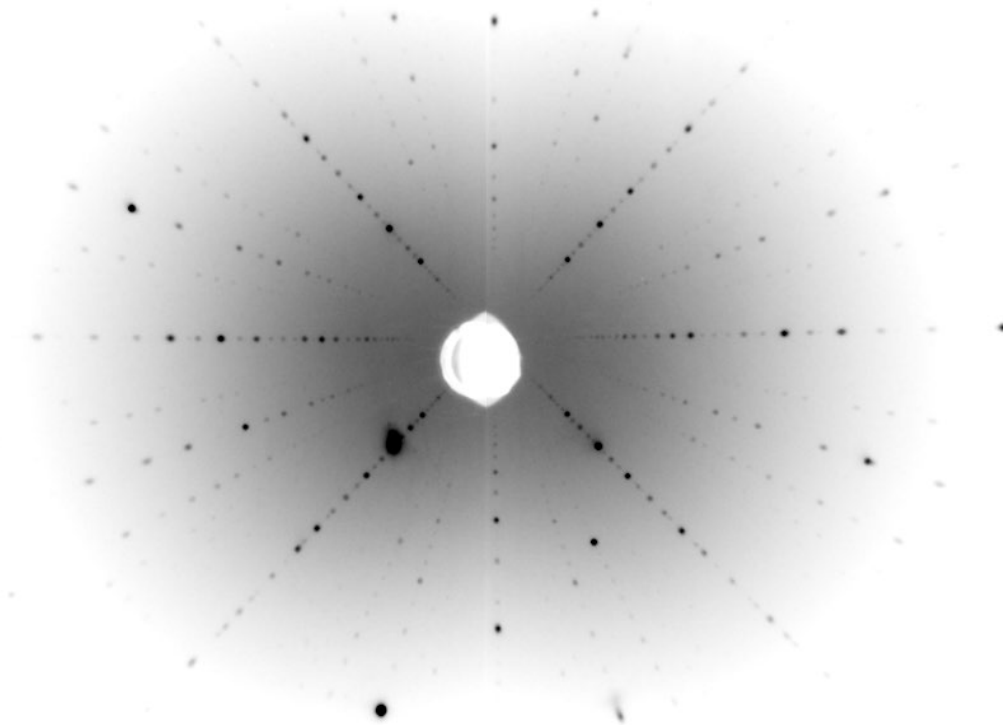


Fig. 1. Typical image of X-ray Laue of the single crystal HoFeO_3 perpendicular to $[010]$ direction, shows the quality of the crystal.

The magnetic field was applied in vertical direction, along b -axis of the crystal, for the measurements it was cooled down in zero field slowly. The measurements of the temperature dependencies of 8 peaks corresponding to four different types of magnetic ordering have been performed in the temperature range 2 – 68 K with 2 K steps while heating for 7 discrete permanent fields: 0.5, 1.25, 2.25, 3.5, 5, 6.5, 8 T. Phase transition process have small temperature hysteresis and temperature of phase transitions may have little difference at heating and cooling.

Crystal structure studies

Powder X-Ray diffraction studies were performed at different temperatures – 300 K, 40 K, 7 K. The refinement of the obtained XRD patterns was performed for space group $Pnma$ (#62) as well as for subgroups of this parent one. For this treatment FullProf suite [29] was used. For all temperatures convergence parameters like χ^2 , R_f did not change noticeably when lower symmetry subgroups were considered. This gives no evidences about lowering of the symmetry. Thus at all temperatures obtained structure (Table 1) should be attributed to space group $Pnma$ (Fig. 2a). The most significant changes in the ions positions observed for oxygen O_1 . Through this anion superexchange interaction along b axis takes place (Fig. 2b). Exchange paths and exchange bond angles for 300 K and 7 K are presented at Table 2. It is noteworthy that both path lengths (d) and bond angles (γ) for exchange through O_1 change their values to a much greater extent than those for exchange through O_2 , corresponding to interaction in ac plane. Interestingly, Fe^{3+} single ion anisotropy constants change their ratio from $A_b < A_{ac}$ at 300 K to $A_b > A_{ac}$ below 35 K [26] that could be connected with such change of superexchange bonds.

Table 1. Crystal structure of HoFeO₃ at 300 K, 7 K, *Pnma*

300 K		$a = 5.5908(1), \quad b = 7.6016(2), \quad c = 5.2778(1), \quad \chi^2 = 2.37$		
		x	y	z
Fe	4(b)	0	0	0.5
Ho	4(c)	0.0680(3)	0.25	0.9790(4)
O _I	4(c)	0.479(2)	0.25	0.077(2)
O ₂	8(d)	0.344(2)	0.058(1)	0.696(2)
7 K		$a = 5.5825(1), \quad b = 7.5845(1), \quad c = 5.2680(1), \quad \chi^2 = 4.31$		
		x	y	z
Fe	4(b)	0	0	0.5
Ho	4(c)	0.0693(3)	0.25	0.9790(5)
O _I	4(c)	0.445(2)	0.25	0.097(3)
O ₂	8(d)	0.319(2)	0.061(1)	0.697(2)

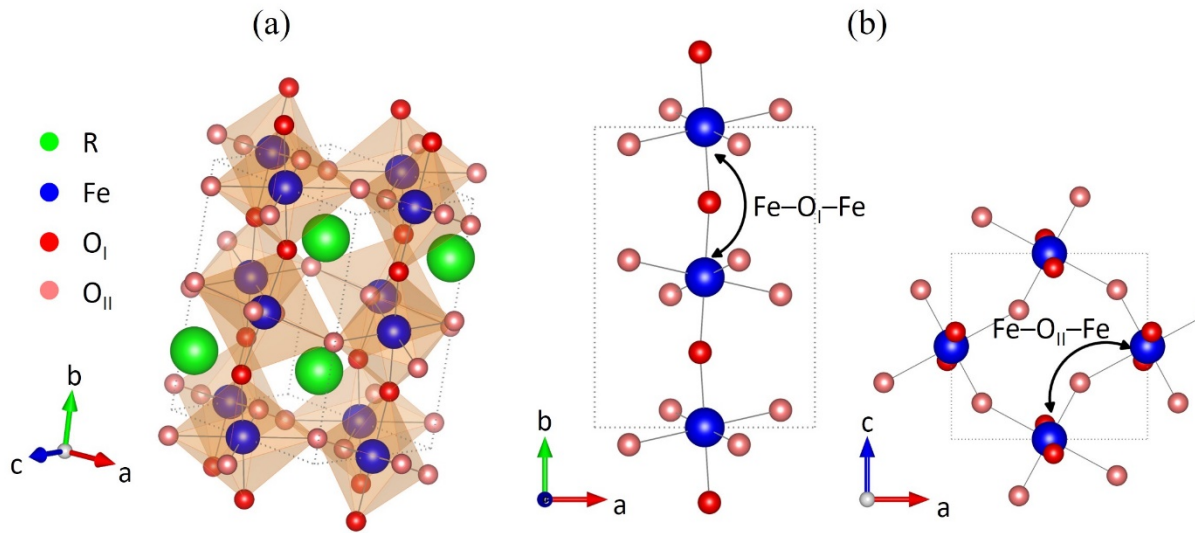


Fig. 2. (a) Crystal structure $RFeO_3$; (b) Exchange paths for the nearest neighbors in Fe sublattice. Configuration Fe–O_I–Fe corresponds to exchange along *c* axis, configuration Fe–O_{II}–Fe – to exchange in *ab* plane.

Table 2. Exchange paths parameters at 300 K, 7 K .

	Fe–O _I –Fe		Fe–O _{II} –Fe	
	d	γ	d	γ
300 K	3.894 (8)	154.9° (7)	4.107 (14)	138.6°(5)
7 K	3.976 (10)	145.1° (9)	4.057 (16)	142.2°(6)

Magnetization studies

Temperature dependence of the magnetization, measured in range 4 – 860 K is presented at Fig. 3a. Magnetization measurements were performed on a single HoFeO₃ crystal with an external magnetic field $H = 1$ kOe, parallel to *b*-axis. As it can be seen, two features present in the obtained

dependence, obviously corresponding to the emergence of a spin-reorientation transition in the temperature range 48 – 58 K and to Neel temperature $T_N \approx 647$ K that is in good agreement with previous works [1, 3]. In order to find possible magnetic transitions in the temperature range of 2 – 100 K, the dependences of $M(T)$ in different magnetic fields were measured (Fig. 3b). It can be seen from Fig. 3b, that a feature corresponding to spin-reorientation transition in the range 48 – 58 K is observed only at field $H = 1$ kOe whereas at large fields, these dependencies become monotonous in this temperature range. The only feature of the $M(T)$ dependence for the field $H = 30$ kOe is the bend at $T = 4.2$ K.

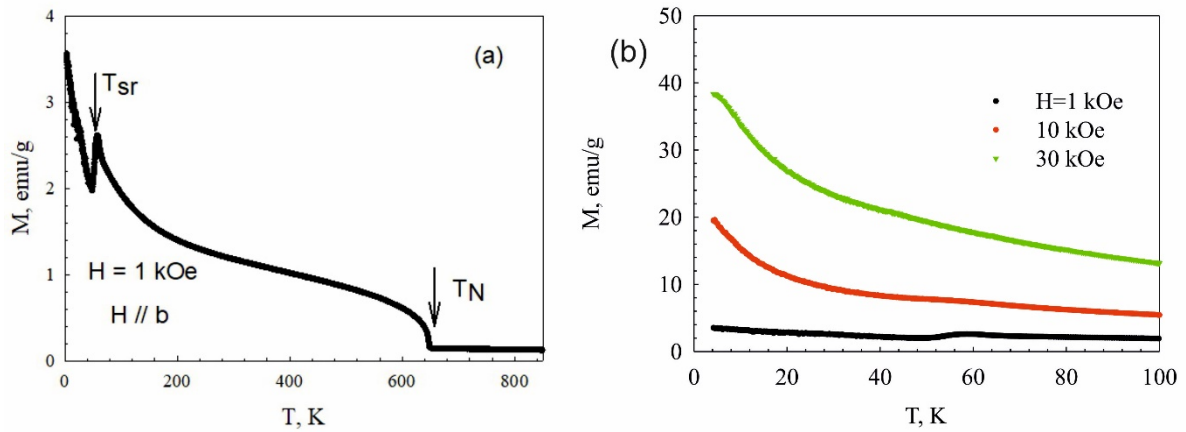


Fig. 3. (a) Temperature dependence of HoFeO₃ single crystal magnetization; (b) – dependences of $M(T)$ in different magnetic fields.

In order to search for new features in the phase diagram of HoFeO₃ in the temperature range of 2 – 100 K we also measured in detail the isotherms of the field dependences of magnetization in this temperature range.

On Fig. 4 the results of measurement data of $M(H)$ in fields up to 90 kOe are presented. It can be seen that the high-field part of $M(H)$ dependence is linear over the entire temperature range

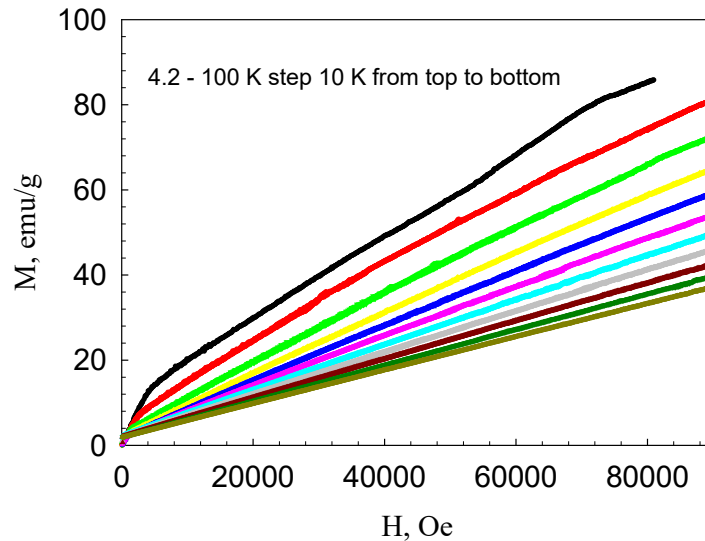


Fig. 4. Field dependence of HoFeO₃ single crystal magnetization at different temperatures.

below and above the spin-reorientation transition. The kink at small fields corresponds to the reorientation of iron, and in high fields the main contribution to the magnetization is made by holmium.

The behavior of the magnetization in the region of the spin-reorientation transition at low magnetic fields was studied in detail, where it is possible to distinguish behavior of iron ions. It was found that dependence $M(H)$ has almost the same behavior well above and below the transition. As can be seen from Fig. 4, for these temperatures $M(H)$ curve is rapidly saturated. A weak slope above saturation corresponds to the influence of paramagnetic holmium. However, in the transition region, the saturation process is more prolonged (for example, pink and blue curves at Fig. 5). This could be the indication of the presence of iron fluctuations in such a transition process and is an interesting fact for further study.

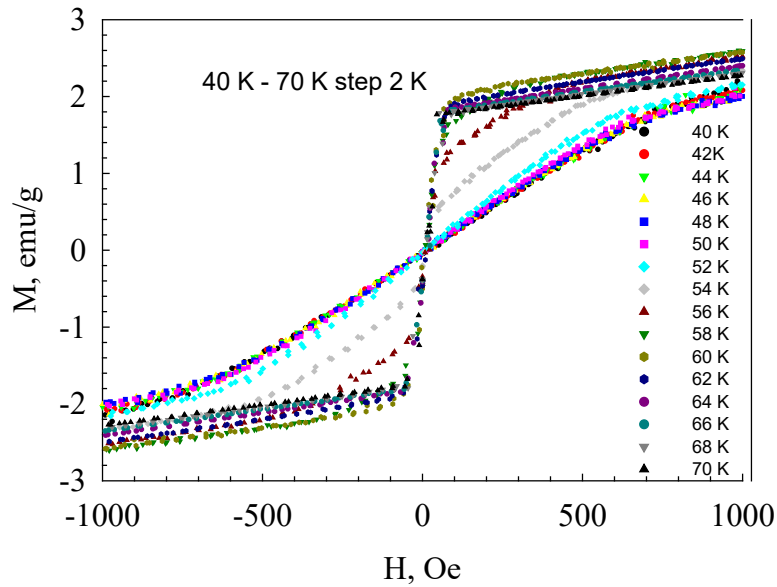


Fig. 5. Field dependence of HoFeO_3 single crystal magnetization in temperature range close to T_{SR} .

At Fig. 6 the results of magnetization measurements in different crystallographic directions at room temperature are presented. The magnetization hysteresis reflects the magnitude of iron ions tilt in different crystallographic directions, which is characteristic of weak ferromagnetism.

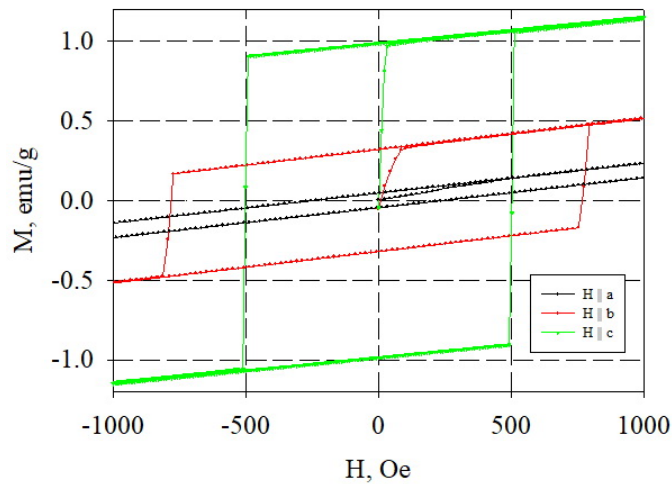


Fig. 6. Field dependence of HoFeO_3 single crystal magnetization at room temperature.

Magnetic symmetry analysis

For the analysis k-SUBGROUPSMAG program [31] from Bilbao Crystallographic Server [32 – 34] was used. Magnetic symmetry of the subgroups of space group $Pnma$ with the propagation vector $\mathbf{k} = 0\ 0\ 0$ can be described by the combination of eight one-dimensional irreducible representations. Their designation in BCS notation is the following: Γ_1^+ , Γ_2^+ , Γ_3^+ , Γ_4^+ , Γ_1^- , Γ_2^- , Γ_3^- , Γ_4^- .

Inside the Fe sublattice the main interaction is the isotropic exchange interaction between the nearest neighbors. Because the crystal cell contains 4 non-equivalent magnetic Fe atoms there are 4 types of possible collinear ordering of the Fe subsystem, which can be expressed by means of the following Bertaut notation [30]:

$$\begin{aligned}\mathbf{F} &= \mathbf{S1} + \mathbf{S2} + \mathbf{S3} + \mathbf{S4}, \\ \mathbf{G} &= \mathbf{S1} - \mathbf{S2} + \mathbf{S3} - \mathbf{S4}, \\ \mathbf{C} &= \mathbf{S1} + \mathbf{S2} - \mathbf{S3} - \mathbf{S4}, \\ \mathbf{A} &= \mathbf{S1} - \mathbf{S2} - \mathbf{S3} + \mathbf{S4},\end{aligned}$$

where \mathbf{G} describes the main antiferromagnetic component of the magnetic structure, \mathbf{F} – vector of ferromagnetism, weak antiferromagnetic components \mathbf{C} and \mathbf{A} describe the canting of the magnetic sublattices. DMI leads to canting of the sublattices and appearance of more complex structures, which can be described using the components of collinear types of ordering. For Fe subsystem, the decomposition of the full magnetic representation Γ^{Fe} has the form:

$$\Gamma^{Fe} = \sum n_v^{Fe} g m_v = 3\Gamma_1^+ \oplus 3\Gamma_2^+ \oplus 3\Gamma_3^+ \oplus 3\Gamma_4^+ \quad (1)$$

And for Ho subsystem full magnetic representation Γ^{Ho} will look like

$$\Gamma^{Ho} = \sum n_v^{Ho} g m_v = 1\Gamma_1^+ \oplus 2\Gamma_1^- \oplus 2\Gamma_2^+ \oplus 1\Gamma_2^- \oplus 2\Gamma_3^+ \oplus 1\Gamma_3^- \oplus 1\Gamma_4^+ \oplus 2\Gamma_4^- \quad (2)$$

In general case the magnetic moment of atom j in cell L with coordinate \mathbf{R} and propagation vectors \mathbf{k} may be written as a Fourier series:

$$\mathbf{m}_j = \sum_{\mathbf{k}} \mathbf{S}_{kj} \cdot e^{-2\pi i \mathbf{k} \mathbf{R}} \quad (3)$$

The vectors \mathbf{S}_{kj} are the Fourier components of the magnetic moments \mathbf{m}_j . They can be written as linear combination of basis functions of irreducible representations:

$$\mathbf{S}_{kj} = \sum_{a,m} C_{a,m} \mathbf{V}_{a,m}(\mathbf{k}, \nu|j) \quad (4)$$

where $C_{a,m}$ are the coefficients of the linear combinations, and basic vectors $\mathbf{V}_{a,m}(\mathbf{k}, \nu|j)$ are constant vectors referred to the basis of the direct cell. The index a varies from 1 up to the dimension of IRs. The index m varies from 1 up to the number corresponding to the number of times the representation Γ_ν is contained in the magnetic reducible representation Γ . By varying these coefficients, one could obtain all the class of magnetic structures corresponding to the symmetry of the propagation vector.

Full magnetic representation will include all irreducible magnetic representations of the subgroups of the parent group #62 for the rare-earth and iron sublattices. Table 3 shows irreducible representations corresponding to magnetic groups and possible type of magnetic ordering for the

sites Fe and Ho. Magnetic groups of lower symmetry within the orthorhombic space group can be described using the direct sum of these representations. For example, magnetic space group $Pnm2_1$ is described by the representation $\Gamma = \Gamma_1^+ \oplus \Gamma_4^-$.

Table 3. The irreducible representations and the corresponding magnetic groups in the $Pnma$ setting.

Irreducible representations	Parent space group $Pnma$		
	Magnetic group	Site of Fe	Site of Ho
Γ_1^+	$Pnma$	$G_x C_y A_z$	C_y
Γ_2^+	$Pn'm'a$	$C_x G_y F_z$	$C_x F_z$
Γ_3^+	$Pnm'a'$	$F_x A_y C_z$	$F_x C_z$
Γ_4^+	$Pn'ma'$	$A_x F_y G_z$	F_y
Γ_1^-	$Pn'm'a'$		$A_x G_z$
Γ_2^-	$Pnma'$		A_y
Γ_3^-	$Pn'ma$		G_y
Γ_4^-	$Pnm'a$		$G_x A_z$

Magnetic scattering dependence on magnetic field

In HoFeO_3 unit cell Fe^{3+} ions occupy special position $4b$ that provides some special conditions for the contribution of different magnetic modes to Bragg reflections with corresponding Miller index parity. Thus to reflections with $h + l$ even, k odd only mode **A** gives contribution, to reflections with k even, $h + l$ odd – only type **C** contributes, $h + l$ even, k even – only type **F**, $h + l$ odd, k odd – only type **G**. For studies, two Bragg reflections for each magnetic mode were chosen: 113 and 311 for type **A**, 201 and 102 for type **C**, 002 and 200 for type **F**, 011 and 110 for type **G**. Temperature dependences of their integral intensities were measured in external magnetic field. For all of these reflections a change in intensity with the temperature was observed. Fig. 7a shows the temperature dependence of reflection 011 intensity for all measured fields and at Fig. 7b the temperature dependence of reflection 201 for fields 0.5 T and 8 T is shown. One can see that the boundaries of the phase transitions shift down in temperature with an increase of external magnetic field. The increase of 011 intensity at zero magnetic field in the temperature range 35 – 50 K definitely is owing to formation of phase Γ_1 , which exists in that temperature range [9]. A dip in intensity of reflection 011 in temperature range of 50 – 55 K appears at field 0.5 T, which was not observed at zero field (Fig. 7a). That means that field leads to the formation of an intermediate phase during the transition below $T_{\text{SR1}} = 53$ K. The increase of intensity still persists at fields 0 – 1.25 T and disappears with further increase in the magnetic field. No increase of 011 intensity below T_{SR1} was observed at fields ≥ 2.25 T, which means that phase Γ_1 is suppressed by the field. A sharp increase in intensity of 201 reflection which indicates an increase of the magnetic moment of holmium shifts to a region of higher temperature (Fig. 7b).

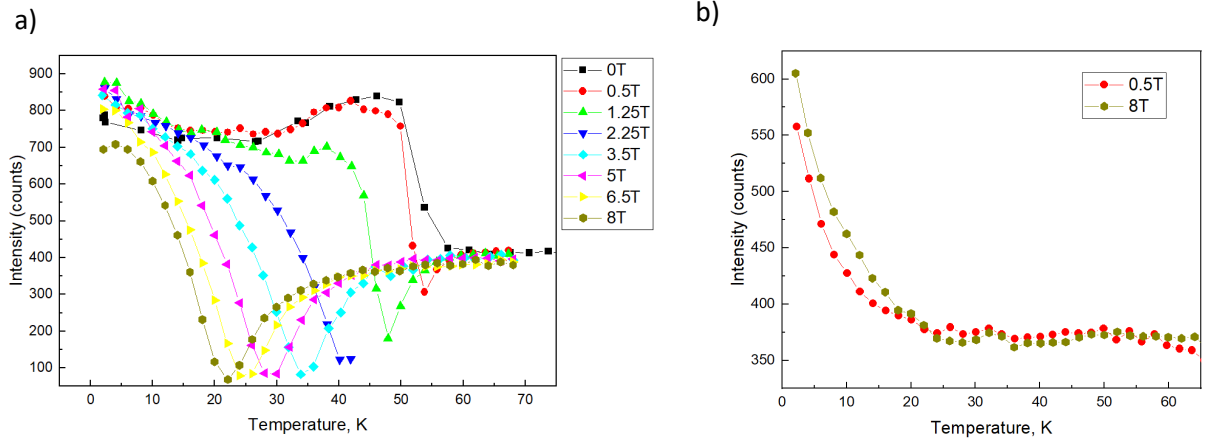


Figure 7. Temperature dependence of the integrated intensities of reflections a) 011 type **G** and b) 201 type **C** in different magnetic fields.

For magnetic structure refinement, we considered magnetic representations shown in Table 1 and results of refinement from work [9]. In this way we obtained set of magnetic phases that can be described by different magnetic representations as well as by different directions and magnitudes of the components of magnetic moments, that follows from the changes in intensity of the corresponding reflections. Resulting phase diagram is shown in Figure 8. Corresponding descriptions of phases are given in Table 4. We consider phases to be different as well in a case if they described by the same set of irreducible presentations but with coefficients $C_{a,m}$ having different signs. Obviously, boundaries between phases are drawn with significant approximation owing to comparatively high e.s.d.s of our magnetic structure refinement.

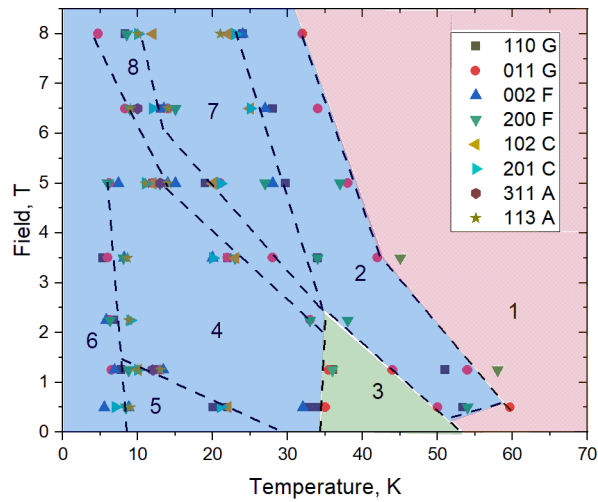


Figure 8. Magnetic phase diagram of HoFeO_3 . Dotted line – phase boundaries. Color area – region that are described by different magnetic representation of the Fe subsystems: red – Γ_4^+ , green – Γ_1^+ , blue – Γ_2^+ . The numbers indicate phases as they are mentioned in the text.

The best fit for phase 2 is obtained using representation $\Gamma = \Gamma_4^+$ with non-zero magnetic moment components of the iron subsystem. But previous studies using polarized neutrons [35] have shown that y -component of the G-type reflections emerges during the transition from phase 1 to phase 3. Also, it was shown that external magnetic field $B = 9$ T at temperature $T = 70$ K induces magnetic moment around $1 \mu_B$ on Ho^{3+} [36]. Therefore, magnetic phase $P2_1'2_1'2_1$ was used to describe the magnetic structure in the fields. This phase is described by representation $\Gamma = \Gamma_2^+ \oplus \Gamma_2^-$ which resolves the existence of y component for G-type reflections and magnetic moments on the Ho^{3+} ions. Groups $Pn'a'2_1$ and $Pn'a2_1'$ are more symmetric groups than $P2_1'2_1'2_1$ and $P2_12_12_1$. Table 4 clearly shows at temperatures above $T_{\text{SR1}} = 53$ K (where only the iron subsystem is ordered) and at temperatures below $T_{\text{NR}} = 10$ K (where the holmium has its own moment alignment) the system is in higher symmetrical phase. In the temperature range $T_{\text{NR}} < T < T_{\text{SR1}}$ various processes take place, which are associated with exchange interactions between the Fe-Ho sublattices and inside the Ho sublattice. At the same time, external field shifts temperature of phase transitions. And, as can be seen from the phase diagram, an increase of external field leads to transitions from the low-symmetry phase (№ 2 or № 3) to highly symmetric phase (№ 1). The same situation was observed in DyFeO_3 where external field leads to transition from phase $P2_12_12_1$ to $Pn'a'2_1$ at temperature around T_{NR} [5]. However, in case of HoFeO_3 this transition goes through an intermediate phase $P2_1'2_1'2_1$.

Table 4. Components of the magnetic moments of the Fe and Ho in different magnetic phases. Magnetic moment values are given in μ_B .

Magnetic representation:		$\Gamma_4^+ \oplus \Gamma_1^-$	$\Gamma_2^+ \oplus \Gamma_2^-$	$\Gamma_1^+ \oplus \Gamma_1^-$	$\Gamma_2^+ \oplus \Gamma_2^-$	$\Gamma_2^+ \oplus \Gamma_2^-$	$\Gamma_2^+ \oplus \Gamma_3^-$	$\Gamma_2^+ \oplus \Gamma_2^-$	$\Gamma_2^+ \oplus \Gamma_2^-$
Magnetic phase		$Pn'a'2_1$	$P2_1'2_1'2_1$	$P2_12_12_1$	$P2_1'2_1'2_1$	$P2_1'2_1'2_1$	$Pn'a2_1'$	$P2_1'2_1'2_1$	$P2_1'2_1'2_1$
Phase number		1	2	3	4	5	6	7	8
Temperature		60 K	40 K	40 K	30 K	15 K	5 K	20 K	11 K
Field		0.5 T	5 T	0.5 T	0.5 T	0.5 T	0.5 T	6.5 T	6.5 T
Fe	Mx	0	0	4.2(1)	0	0	0	0	0
	My	-0.7(2)	-3.3(4)	0	-4.5(1)	-4.8(3)	-5.2(9)	-3.3(3)	-4.3(8)
	Mz	-4.23(8)	-1.8 (7)	1.2(5)	0.2 (5)	0.2 (5)	0.2 (5)	-2.6(9)	-1.1(6)
Ho	Mx	0	1.7(8)	-0.8(3)	2.2(6)	2.1(2)	5.4(1)	2.6(8)	3.4(2)
	My	0	0	0	0.9(6)	1.4(3)	0	0	0.4(5)
	Mz	0	0	-0.3(2)	1.6(5)	-2.3(3)	3.3(2)	-2.1(1.0)	1.0(6)
R factor		1.12	4.41	1.81	2.18	0.96	1.20	5.40	0.86

Phase transitions in weak magnetic fields

With external magnetic field full magnetic Hamiltonian for HoFeO_3 will have form:

$$H = H^{Fe-Fe} + H^{Fe-Ho} + H^{Ho-Ho} + H_{ext} \quad (5)$$

Complex interplay, balance and competition of these interactions provide observed sequence of phase transitions. In the phase 1 (configuration Γ_4) the interactions within Ho subsystem and between Ho and Fe subsystems could be neglected. In the absence of external field, Ho^{3+} ions are in the exchange field of Fe^{3+} ordered subsystem, which induces magnetic moment on the holmium ions. At temperature around $T_{\text{SR1}} = 53$ K, the exchange interactions and easy-plane anisotropy in ac plane play a main role inside the iron subsystem [26]. The strongest superexchange interaction is along the iron chains: $J_b = 4.9$ meV, interaction in ac plane is weaker: $J_{ac} = 4.76$ meV [26].

However, the easy-plane anisotropy stabilizes the system and the moments of iron sublattice lie in the ac plane with small canting due to DMI. At T_{SR1} exchange interaction Fe-Ho increases to a level sufficient to rotate Fe moment in ac plane that gives Γ_1 structure – phase 3 in our notation.

It can be seen that already in a weak magnetic field above 0.5 T along b axis HoFeO_3 has an additional intermediate phase and transitions are shifted to the low temperature. It is logical to assume that external field induces an additional ordered magnetic moment on Ho^{3+} ions that in turn produces an addition to exchange interaction $J_{ij}^{\text{Fe-Ho}}$ between sublattices Fe and Ho. The increase of Fe-Ho exchange interaction produced by field 0.5 T provides the transition from phase 1 to phase 2. This is clearly seen at the temperature dependence of reflection 011 as a fall of its intensity, which takes place due to rotation of Fe magnetic moment in the direction to b axis. Magnetic field higher than 0.5 T influences on iron sublattice much stronger, leading to the essential changes in the alignment of Fe moments. In this case iron sublattice produces field opposite to the external one. Therefore, the temperature of transition from phase 1 to phase 2 decreases with the field increase. Behavior of Ho magnetic moments reflects the competition between external magnetic field and internal field from the Fe-sublattice. At low external field, the main influence on Ho sublattice is exerted by field from Fe-sublattice thus interaction $J_{ij}^{\text{Fe-Ho}}$ rotates the iron magnetic moments from phase 1 to phase 3 through b direction (see Fig. 9).

Since holmium has a highly anisotropic g-factor ($g_x = 6.7$, $g_y = 1.6$, $g_z = 3.5$) [37], at fields higher than $B = 2.5$ T, external field holds the Ho moments along x direction mainly and the anisotropic interaction $J_{ij}^{\text{Fe-Ho}}$ holds the iron magnetic moment close to b axis. Thus phase 3 is suppressed by the field.

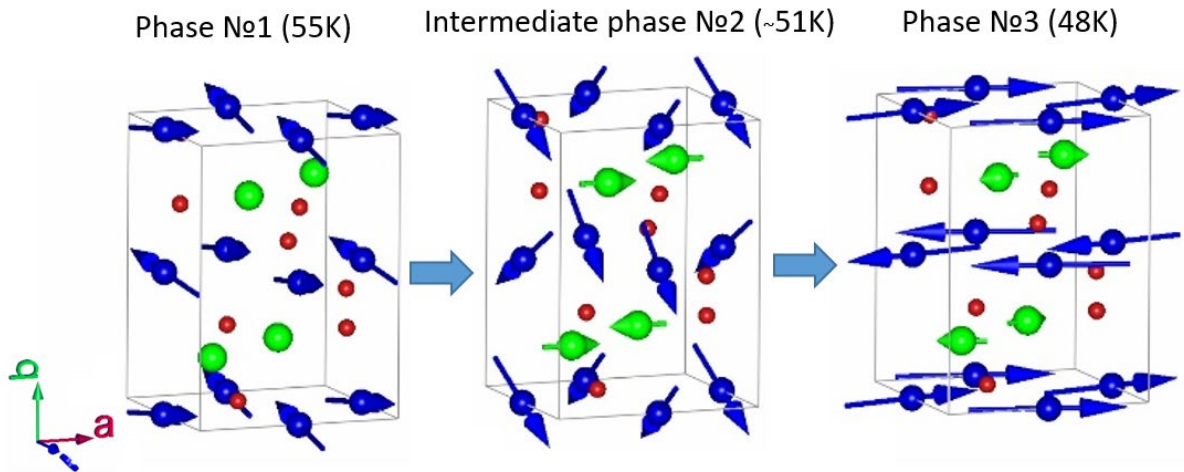


Figure 9. Scheme of magnetic structure evolution by the reorientation phase transition in HoFeO_3 near 50 K with magnetic field 0.5 T along $[010]$.

Low temperature phase transitions

At the temperature $T_{SR2} = 35$ K the increase of induced magnetic moment of Ho subsystem provides subsequent increase of exchange interaction J_{mn}^{Ho} which leads to a new redistribution of the energy balance. This gives new phase - phase 4, where Fe^{3+} moments turn closer to b direction and system described by magnetic representation $\Gamma = \Gamma_2^+ \oplus \Gamma_2^-$ as well as for phase 2, but with more distinct contribution from Ho subsystem. Below T_{SR2} exchange interactions Ho-Ho and Ho-Fe should be necessary taken in account:

$$H^{Fe-Ho} + H^{Ho-Ho} = \sum_{ij} S_i^{Fe} \cdot J_{ij}^{Fe-Ho} \cdot s_j^{Ho} - \sum_{mn} s_m^{Ho} \cdot J_{mn}^{Ho} \cdot s_n^{Ho} \quad (6)$$

$$+ \sum_{ij} D_{ij}^{Fe-Ho} \cdot (S_i^{Fe} \times s_j^{Ho}) - \sum_{mn} D_{mn}^{Ho-Ho} \cdot (s_m^{Ho} \times s_n^{Ho}) \sum_i s_i^{Ho} \cdot \mathbf{H}_{ext}$$

where J_{ij} – isotropic exchange, \mathbf{D}_{ij}^{N-M} – Dzyaloshinsky vectors which could consist of antisymmetric exchange and single ion anisotropy, \mathbf{S}_i^{Fe} – effective spin operator of Fe, \mathbf{s}^{Ho} – the Ho spin moment operator:

$$\mathbf{s}^{Ho} = (g_j - 1)\mathbf{J} \quad (7)$$

where g_j – Lande factor, \mathbf{J} – total angular moment.

As it has been established, exchange interactions Ho-Ho and Ho-Fe have different signs [26]. Increase of the ordered magnetic moment on holmium ions leads to increase of the contribution to energy from exchange Ho-Ho. The equality of Ho-Ho and Ho-Fe interactions, probably, is the reason of transition at $T = 24$ K (in this work, and $T = 20$ K in [9]) to the phase 5, where direction of the ferromagnetic component of Ho changes sign (see Fig. 10a).

Magnetic field above 1 T destroys this balance, that suppresses this phase also (Fig. 10b). At temperature $T_{NR} = 10$ K Ho^{3+} spontaneous magnetic ordering takes place. It leads to new rebalancing of the energy: the exchange interaction within rare-earth subsystem is already strong enough to hold its magnetic moment mainly along Ho^{3+} easy axis x and not to follow the influence of iron sublattice and external field. Therefore, below $T_{NR} = 10$ K Ho^{3+} moment aligns along hard axis $m_y \approx 0$, and the ferromagnetic component m_z of Ho^{3+} changes sign again (phase 6, Fig. 10a).

As it can be seen, field above 2 T makes significant influence on Ho-sublattice. At field $B = 2.5$ T energy of magnetic field is higher than energy of Fe-Ho interaction. In this way, at temperature above 35 K, phase 3 disappears. At the same time, the external field with value higher than 2 T is strong enough to induce y component of the magnetic moment of the Ho^{3+} ions. In this way new phase 7 with strong canting of Fe sublattice is formed.

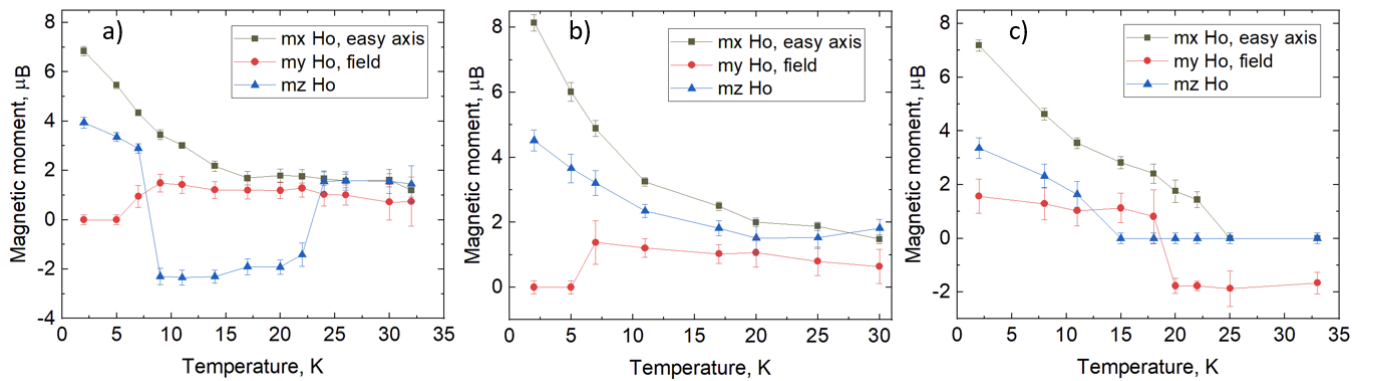


Figure 10. Temperature dependence of the x , y and z components of Ho magnetic moments in the field a) 0.5 T, b) 1.25 T and c) 5 T.

Phase 8 is intermediate phase, where the Fe moments have strong moment along b axis with significant ferromagnetic component along c . Field above 4 T leads to canting of Ho sublattice

moments and gives a non-zero y -component of Ho magnetic moment (Fig. 10c). Magnetic structures corresponding to different magnetic phases at 20 K are shown on Figure 11.

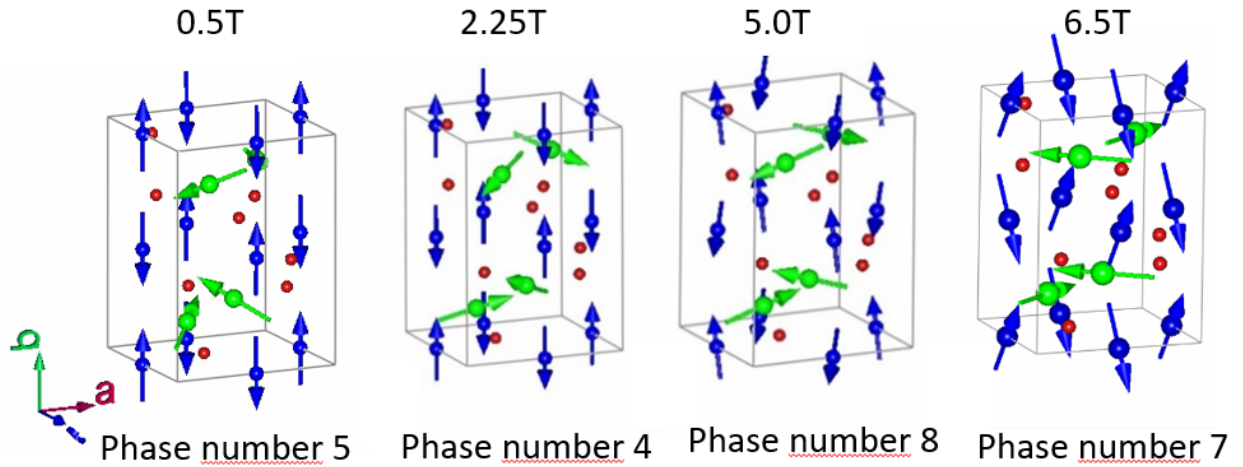


Figure 11. Schematic representation of the magnetic structure at temperature $T = 20$ K with increasing magnetic field ($B \parallel b$).

Conclusion

Our studies demonstrate that HoFeO_3 has a rich phase diagram in an external magnetic field. The competition between the external magnetic field, the antisymmetric DMI and isotropic exchange interactions between Fe and Ho sublattice and inside Fe sublattice leads to a complex picture of phase transitions in rare-earth orthoferrite HoFeO_3 . According to our consideration we can outline 8 different magnetic phases, produced or suppressed by the field. This is the result of the balance of exchange interactions inside crystal and external magnetic field. Such complex behavior may cause the useful functionality of rare-earth orthoferrites. The obtained results are in good agreement with the work on inelastic neutron scattering, where the values of exchange interactions were calculated and with measurements of magnetic entropy change where peaks of ΔS_M lie near the spin reorientation transition between phases 1 or 2 and 3; phases 4, 5 and 6.

Acknowledgments

This work was supported by the Russian Foundation for Basic Research grant # 19-52-12047, and DFG grant # SA 3688/1-1. Neutron Experiments were performed at the instrument POLI jointly operated by RWTH Aachen University and Forschungszentrum Jülich at MLZ within JARA-FIT collaboration.

References

- [1] W.C. Koehler, E.O. Wollan, M.K. Wilkinson, Phys. Rev. 118 (1960) 58.
- [2] M. Marezio, J.P. Remeika, P.D. Dernier, Acta Cryst. B 26 (1970) 2008.
- [3] R. White, J. Appl. Phys. 40 (1969) 1061.
- [4] K. Park, H. Sim, J. C Leiner, Y. Yoshida, J. Jeong, S. Yano, J. Gardner, P. Bourges, M. Klicpera, V. Sechovský, M. Boehm and J. Park, J. Phys.: Condens. Matter 30 (2018)
- [5] Y. Tokunaga, S. Iguchi, T. Arima, and Y. Tokura, Phys. Rev. Lett. 101, 097205 (2008)

- [6] S. Chaturvedi, P. Shyam, A. Apte, J. Kumar, A. Bhattacharyya, A. M. Awasthi, and S. Kulkarni, PHYSICAL REVIEW B 93, 174117 (2016)
- [7] A. Bombik, B. Leśniewska, A.W Pacyna, JMMM, 214, 243 (2000)
- [8] L. T. Tsymbal, et al. Low Temp. Phys. 31 (3–4), March–April 2005
- [9] T. Chatterji, M. Meven, P.J. Brown, AIP Adv. 7 (2017) 045106.
- [10] Artyukhin, S., Mostovoy, M., Jensen, N. et al. Solitonic lattice and Yukawa forces in the rare-earth orthoferrite TbFeO₃. Nature Mater 11, 694–699 (2012).
- [11] A.K. Zvezdin, A.A. Mukhin, JETP Lett. 88 (2008) 505.
- [12] Y. Tokunaga, et al., Nat. Mat. 8 (2009) 558.
- [13] B. Rajeswaran et al., (2013) EPL 101 17001
- [14] K. Dey, A. Indra, S. Mukherjee, S. Majumdar, J. Stremper, O. Fabelo, E. Mossou, T. Chatterji, and S. Giri. Phys. Rev. B 100, 214432 – Published 26 December 2019
- [15] J.-H. Lee, Y.K. Jeong, J.H. Park, M.-A. Oak, H.M. Jang, J.Y. Son, J.F. Scott, Phys. Rev. Lett. 107 (2011) 117201.
- [16] P. Mandal, V.S. Bhadrani, Y. Sundarayya, C. Narayana, A. Sundaresan, C.N.R. Rao, Phys. Rev. Lett. 107 (2011) 137202.
- [17] U. Chowdhury, S. Goswami, D. Bhattacharya, J. Ghosh, S. Basu, S. Neogi, Appl. Phys. Lett. 105 (2014) 052911.
- [18] I. E. Dzyaloshinsky, J. Phys. Chem. Solids 4 (1958) 241.
- [19] T. Moriya, Phys. Rev. 120 (1960) 91.
- [20] Ke, Y.-J., Zhang, X.-Q., Ma, Y. et al., Sci Rep 6, 19775 (2016)
- [21] M. Shao et al., Solid State Communications 152 (2012) 947–950
- [22] A. Bhattacharjee, K. Saito, M. Sorai, J. Phys. Chem. Solids 63 (2002) 569.
- [23] M. Shao, S. Cao, Y. Wang, S. Yuan, B. Kang, J. Zhang, A. Wu, J. Xu, J. Cryst. Growth 318 (2011) 947.
- [24] O. Nikolov, I. Hall, K.W. Godfrey, J. Phys. Condens. Matter 7 (1995) 4949.
- [25] S.N. Barilo, A.P. Ges, S.A. Guretskii, D.I. Zhigunov, A.A. Ignatenko, A.N. Igumentsev, I.D. Lomako, A.M. Luginets, J. Crystal Growth 108 (1991) 314
- [26] A.K.Ovsyanikov, I.A.Zobkalo, W.Schmidt, S.N.Barilo, S.A.Guretskii, V.Hutanu, JMMM, Volume 507, 1 (2020)
- [27] V. Huțanu, M. Meven, E. Lelièvre-Berna, G. Heger, Physica B 404, 2633–2636 (2009)
- [28] V. Hutanu, Journal of large-scale research facilities 1, A16 (2015).
- [29] J. Rodriguez-Carvajal, Physica B 192, 55 (1993).
- [30] E. F. Bertaut, Magnetism (Academic, New York, 1963).
- [31] J.M. Perez-Mato, S.V. Gallego, E.S. Tasci, L. Elcoro, G. de la Flor, and M.I. Aroyo, Annu. Rev. Mater. Res. (2015)
- [32] M. I. Aroyo, J. M. Perez-Mato, D. Orobengoa, E. Tasci, G. de la Flor, A. Kirov, Bulg.

Chem. Commun. 43(2) 183-197 (2011)

[33] M. I. Aroyo, J. M. Perez-Mato, C. Capillas, E. Kroumova, S. Ivantchev, G. Madariaga, A. Kirov & H. Wondratschek, Z. Krist. 221, 1, 15-27 (2006)

[34] M. I. Aroyo, A. Kirov, C. Capillas, J. M. Perez-Mato & H. Wondratschek, Acta Cryst. A62, 115-128 (2006)

[35] A. Ovsianikov et al., "Breaking the magnetic symmetry by reorientation transition near 50 K in multiferroic magnetocaloric HoFeO₃," in IEEE Transactions on Magnetics, doi:10.1109/TMAG.2021.3082324.

[36] T Chatterji et al 2017 J. Phys.: Condens. Matter 29 385802

[37] Schuchert, H., Hüfner, S. & Faulhaber, Z. Physik 220, 280–292 (1969)